# VERTICAL OVERHUNG ROTOR DYNAMICS WITH IMPACT

**Fredy Jonel Coral Alamo**
Pontifícia Universidade Católica do Rio de Janeiro
Rua Marquês de São Vicente, 225 – Gávea
Rio de Janeiro – RJ – Brasil, 22453-900
fjcoral@mec.puc-rio.br

**Hans Ingo Weber**
Pontifícia Universidade Católica do Rio de Janeiro
Rua Marquês de São Vicente, 225 – Gávea
Rio de Janeiro – RJ – Brasil, 22453-900
hans@mec.puc-rio.br

***Abstract.*** *The purpose of this work is to analyze the overhung rotor dynamics considering the contact phenomenon between the disk and an annular ring. The analysis of contact is particularly complex, due to the high nonlinearity of the motion equations. The impact is accounted by a consistent contact model, the Kelvin-Vôigt model. Motion equation for the rotor is encountered employing the Lagrangean method.; These equations are capable of capturing phenomena due to lateral vibration, like: forward whirl, backward whirl, rolling or sliding along the annular ring. Due to the combined parameters and the effect of nonlinearity in the motion equations, the dynamical response is not simple or easily predictable. Numerical simulation is the preferred method of analysis, here it is used the Runge-Kutta Fehlberg method. Simulation results show that under certain conditions, the rotor changes its orbit due to the impacts with the annular ring and after that, it executes backward whirl motion. It is a kind of phenomenon which is considered as the most violent and dangerous in rotating machines. The passing through its critical speed is analyzed when driven by an electric motor (also when the system operates under a constant rotational velocity). In addition in this work, the results obtained with an experimental test rig are used to investigate the whirl phenomenon.*

***Keywords.*** *Rotor Dynamics; Rolling and Sliding; Forward and Backward Whirl; Impact.*

## 1. Introduction

The study of rotating machines has special importance for industries, due to the huge amount of applications. One of these applications is in oil well drilling, where, the overhung rotor model may represent, satisfactorily, the lateral dynamics of a drillstring section when it is impacting with the wall. Jansen (1993) models a drill collar section (between two stabilizers) as a rotating shaft, supported in two bearings. Only the first bending mode of the collar section is taken in account, and therefore the model reduces to a mass-spring system constrained to move in a plane perpendicular to the borehold axis. Melakhessou et al. (2003) study the local contact between the drillstring and the well during drilling operations, they use the model proposed by Jansen (1993) that considers the drillstring as an unbalanced rotor supported by two bearings.

If there is a rotor-stator system with impact, the rotor lateral vibration may be induced by the friction existing between the rotor and stator: this interaction may origin a forward whirl motion in the rotor, along the stator. On the other hand, if we have an unbalanced rotating system without impact, the forward whirl motion can be induced by introducing stiffness or damping asymmetry in the system, Atalla (1991).

The impact is a complex phenomenon that is still under investigation; a recent work by Schiehlen (2003) shows that the method of multibody systems is most efficient for the dynamical analysis of machines and structures. During impact, kinetic energy is lost by plastic deformations, viscoelastic effects and wave propagation. For rigid body models, like Brach's model (1998), the energy loss is measured macromechanically by the coefficient of restitution. In this work it is used a vibroimpact model, Rajalingham & Rakheja (2000), which represents satisfactorily the impact phenomenon, where the impact force behavior is parabolic.

In order to investigate the dynamics of the system, the equation of motion for the rotor is obtained by the Lagrange approach, and it is solved numerically using the $5^{th}$ order Runge-Kutta Fehlberg method. Finally, numerical results are compared with those obtained from the experimental test rig and related literature.

## 2. Motion Equations

For the system shown in Fig. (1), the motion equation is obtained for two cases: one when the impacting system is accelerating, and, other with constant rotational velocity. When the rotating disk impacts against the ring, impact forces acting on the disk are considered. In order to calculate the impact force, it is used here the vibroimpact model for the normal force and the Coulomb's law for the tangential force.

### 2.1. Lagrangean Approach

This approach is developed using two scalar magnitudes, energy and work. For the system showed in Fig. (1) we have 4DOF: a rigid body rotation of the motor shaft $(\theta)$, a torsional deformation $(\phi)$ of the rotor shaft and two orthogonal lateral deflections of the disk center $(x, y)$.

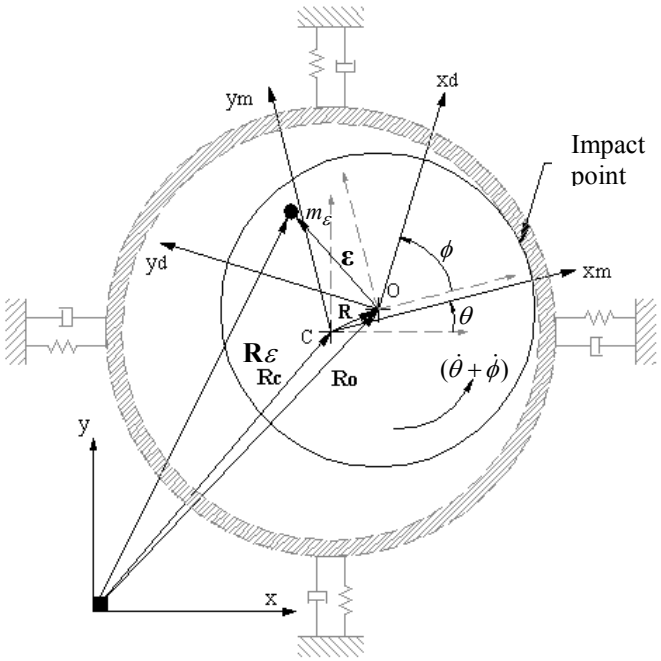


Figure 1. Deformed state and DOF of the system.

In Fig. (1) there are three coordinate systems: $(x, y)$ are inertial coordinates, $(x_m, y_m)$ are rotating coordinates attached to the motor shaft and $(x_d, y_d)$ are rotating coordinates attached to the disk, $m_\varepsilon$ represents the disk imbalance that is located by the vector $\boldsymbol{\varepsilon} = \begin{bmatrix} \varepsilon_x & \varepsilon_y \end{bmatrix}^T$ with respect to the disk coordinate system $(x_d, y_d)$. The disk and ring geometric centers are defined by the position vector $\mathbf{R}_0 = \begin{bmatrix} x & y \end{bmatrix}^T$ and $\mathbf{R}_c = \begin{bmatrix} X & Y \end{bmatrix}^T$, respectively.

To develop the motion equations, the Lagrange equation for a non-conservative system is used here:

$$\frac{d}{dt}\left(\frac{\partial T}{\partial \dot{q}_i}\right) - \frac{\partial T}{\partial q_i} + \frac{\partial U}{\partial q_i} + \frac{\partial \Re}{\partial \dot{q}_i} = Q_i \qquad i = 1, 2, \ldots n$$
$$\frac{\partial \Re}{\partial \dot{q}_i} = \sum_{s=1}^{n} c_{is}\dot{q}_s \tag{1}$$

In Eq. (1), $T$ and $U$ are the Kinetic and Potential Energy; $\Re$ is the Rayleigh's energy dissipation function; $Q_i$ are the generalized forces associated with the generalized coordinates $q_i = \begin{bmatrix} x & y & \theta & \phi \end{bmatrix}$.

The expression for the **Kinetic Energy** is:

$$T = \frac{1}{2}m_d\left(\dot{x}^2 + \dot{y}^2\right) + \frac{1}{2}J\left(\dot\theta + \dot\phi\right)^2 + \frac{1}{2}J_m\left(\dot\theta\right)^2 + \frac{1}{2}m_\varepsilon\left(\dot{\mathbf{R}}_\varepsilon{}^T\dot{\mathbf{R}}_\varepsilon\right) \tag{2}$$

Here, the first term is the translational energy of the disk, the second is the rotational energy of the rotor, the third is the rotational energy of the electric motor shaft, and, the last one is the imbalance energy.

The location of $m_\varepsilon$ in the inertial system $(x, y)$ is given by: $\mathbf{R}_\varepsilon = \mathbf{R}_0 + \mathbf{A}_{(\theta+\phi)}\boldsymbol{\varepsilon}$ where: $\boldsymbol{\varepsilon} = \begin{bmatrix} \varepsilon_x & \varepsilon_y \end{bmatrix}^T$, and $\mathbf{A}(\theta+\phi) = \begin{bmatrix} \cos(\theta+\phi) & -\text{sen}(\theta+\phi) \\ \text{sen}(\theta+\phi) & \cos(\theta+\phi) \end{bmatrix}$ is responsible for the transformation of coordinates $(x, y) \xrightarrow{(\theta+\phi)} (x_d, y_d)$.

Finally the derivative of $\mathbf{R}_\varepsilon$ is define by:

$$\dot{\mathbf{R}}_\varepsilon = \dot{\mathbf{R}}_0 + (\dot\theta + \dot\phi)\begin{bmatrix} -\text{sen}(\theta+\phi) & -\cos(\theta+\phi) \\ \cos(\theta+\phi) & -\text{sen}(\theta+\phi) \end{bmatrix}\boldsymbol{\varepsilon} \tag{3}$$

Replacing Eq. (3) into Eq. (2), the Kinetic Energy results:

$$T = \frac{1}{2}m_d\left(\dot{x}^2+\dot{y}^2\right)+\frac{1}{2}J\left(\dot{\theta}+\dot{\phi}\right)^2+\frac{1}{2}J_m\left(\dot{\theta}\right)^2+\frac{1}{2}m_\varepsilon\left[\left(\dot{\theta}+\dot{\phi}\right)\left(-\varepsilon_x\,\mathrm{sen}(\theta+\phi)-\varepsilon_y\cos(\theta+\phi)\right)+\dot{x}\right]^2+ \frac{1}{2}m_\varepsilon\left[\left(\dot{\theta}+\dot{\phi}\right)\left(-\varepsilon_y\,\mathrm{sen}(\theta+\phi)+\varepsilon_x\cos(\theta+\phi)\right)+\dot{y}\right]^2 \tag{4}$$

The expression for the **Potential Energy** is:

$$U = \frac{1}{2}k_b x^2+\frac{1}{2}k_b y^2+\frac{1}{2}k_t\phi^2 \tag{5}$$

Here, the first and second terms are the energy due to shaft flexion and the last one is due to shaft torsion.

The expressions for the **Rayleigh's Energy Dissipation Function**, considering viscous damping, proportional and non coupled, are:

$$\frac{\partial\Re}{\partial\dot{x}} = c_{xx}\dot{x},\quad \frac{\partial\Re}{\partial\dot{y}} = c_{yy}\dot{y},\quad \frac{\partial\Re}{\partial\dot{\theta}} = 0 \quad \text{e} \quad \frac{\partial\Re}{\partial\dot{\phi}} = c_{\phi\phi}\dot{\phi} \tag{6}$$

Where, $c_{xx} = c_{yy} = c_b$ and $c_{\phi\phi} = c_t$ are the flexural and torsional damping coefficients, respectively.

Considering that the vector of generalized forces, for 4DOF, is given by: $\mathbf{Q} = \begin{bmatrix} Q_x & Q_y & Q_\theta & Q_\phi \end{bmatrix}^T$, and, using the Lagrange equation, Eq. (1), results in the next four equations for the variables $(x, y, \theta, \phi)$, respectively:

$$(m_d+m_\varepsilon)\ddot{x}+m_\varepsilon(\ddot{\theta}+\ddot{\phi})[-\varepsilon_x\,\mathrm{sen}(\theta+\phi)-\varepsilon_y\cos(\theta+\phi)]+ m_\varepsilon(\dot{\theta}+\dot{\phi})^2[-\varepsilon_x\cos(\theta+\phi)+\varepsilon_y\,\mathrm{sen}(\theta+\phi)]+c_b\dot{x}+k_b x = Q_x \tag{7}$$

$$(m_d+m_\varepsilon)\ddot{y}+m_\varepsilon(\ddot{\theta}+\ddot{\phi})[\varepsilon_x\cos(\theta+\phi)-\varepsilon_y\,\mathrm{sen}(\theta+\phi)]+ m_\varepsilon(\dot{\theta}+\dot{\phi})^2[-\varepsilon_x\,\mathrm{sen}(\theta+\phi)+\varepsilon_y\cos(\theta+\phi)]+c_b\dot{y}+k_b y = Q_y \tag{8}$$

$$m_\varepsilon[-\varepsilon_x\,\mathrm{sen}(\theta+\phi)-\varepsilon_y\cos(\theta+\phi)]\ddot{x}+m_\varepsilon[+\varepsilon_x\cos(\theta+\phi)- \varepsilon_y\,\mathrm{sen}(\theta+\phi)]\ddot{y}+[J_m+J+m_\varepsilon\varepsilon^2]\ddot{\theta}+[J+m_\varepsilon\varepsilon^2]\ddot{\phi} = Q_\theta \tag{9}$$

$$m_\varepsilon[-\varepsilon_x\,\mathrm{sen}(\theta+\phi)-\varepsilon_y\cos(\theta+\phi)]\ddot{x}+m_\varepsilon[+\varepsilon_x\cos(\theta+\phi)- \varepsilon_y\,\mathrm{sen}(\theta+\phi)]\ddot{y}+[J+m_\varepsilon\varepsilon^2]\ddot{\theta}+[J+m_\varepsilon\varepsilon^2]\ddot{\phi}+c_t\dot{\phi}+k_t\phi = Q_\phi \tag{10}$$

Arranging these equations in matrix form $\mathbf{M}\ddot{\mathbf{Z}}+\boldsymbol{\zeta}\dot{\mathbf{Z}}+\mathbf{K}\mathbf{Z}+\mathbf{P} = \mathbf{Q}$, it gives:

$$\begin{bmatrix} m_1 & 0 & m_2 & m_2 \\ 0 & m_1 & m_3 & m_3 \\ m_2 & m_3 & m_4 & m_5 \\ m_2 & m_3 & m_5 & m_5 \end{bmatrix}\begin{bmatrix}\ddot{x}\\ \ddot{y}\\ \ddot{\theta}\\ \ddot{\phi}\end{bmatrix}+\begin{bmatrix} c_b & 0 & 0 & 0 \\ 0 & c_b & 0 & 0 \\ 0 & 0 & 0 & 0 \\ 0 & 0 & 0 & c_t \end{bmatrix}\begin{bmatrix}\dot{x}\\ \dot{y}\\ \dot{\theta}\\ \dot{\phi}\end{bmatrix}+\begin{bmatrix} k_b & 0 & 0 & 0 \\ 0 & k_b & 0 & 0 \\ 0 & 0 & 0 & 0 \\ 0 & 0 & 0 & k_t \end{bmatrix}\begin{bmatrix} x\\ y\\ \theta\\ \phi\end{bmatrix}+\begin{bmatrix} P_x\\ P_y\\ 0\\ 0\end{bmatrix}=\begin{bmatrix} Q_x\\ Q_y\\ Q_\theta\\ Q_\phi\end{bmatrix} \tag{11}$$

The mass matrix elements are:

$m_1 = m_d+m_\varepsilon$

$m_2 = -m_\varepsilon\left[\varepsilon_x\,\mathrm{sen}\left(\theta+\phi\right)+\varepsilon_y\cos\left(\theta+\phi\right)\right]$

$m_3 = +m_\varepsilon\left[\varepsilon_x\cos\left(\theta+\phi\right)-\varepsilon_y\,\mathrm{sen}\left(\theta+\phi\right)\right]$

$m_4 = m_\varepsilon\varepsilon^2+J+J_m$

$m_5 = m_\varepsilon\varepsilon^2+J$

The non-linear forces, which represent the centrifugal forces, are:

$$P_x = -m_\varepsilon \left(\dot{\theta}+\dot{\phi}\right)^2 \left[\varepsilon_x \cos\left(\theta+\phi\right) - \varepsilon_y \operatorname{sen}\left(\theta+\phi\right)\right]$$

$$P_y = -m_\varepsilon \left(\dot{\theta}+\dot{\phi}\right)^2 \left[\varepsilon_x \operatorname{sen}\left(\theta+\phi\right) + \varepsilon_y \cos\left(\theta+\phi\right)\right]$$

In Eq. (11), we can see that the mass matrix is a non-singular matrix, $|\mathbf{M}| = J_m(m_d + m_\varepsilon)(m_d J + m_d m_\varepsilon \varepsilon^2 + m_\varepsilon J)$, and then, we will not have any singularity problems when the motion equation is solved numerically.

### 2.2. Motion with Impact

When the disk center displacement is greater than the radial gap $(\delta)$ between the disk and the ring, there will appear impact forces on the disk: normal and tangential. The normal impact force $F_n$ is calculated modeling the radial deformation at the contact point; along the duration of the impact; it is assumed the Kelvin-Vôigt arrangement (a spring and damper in parallel), the spring represents the contact rigidity $K_C$ and the damper represents the contact damper coefficient $C_C$. The tangential impact force $F_t$ arises because the system is rotating and there is a friction coefficient between the surfaces in contact, this force is computed using Coulomb's law, where, the product between the normal force and the assumed friction coefficient gives the tangential force, $F_t = \mu F_n$.

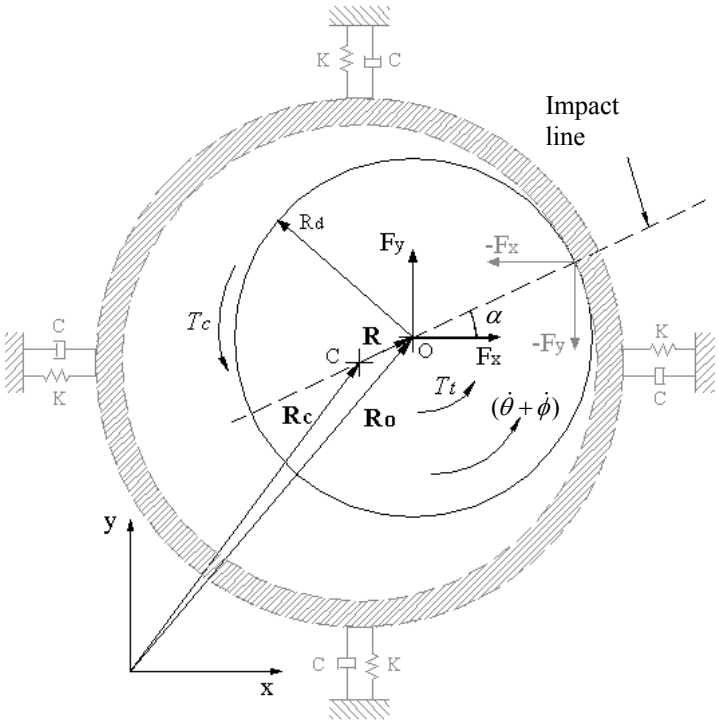


Figure 2. Impacting forces on the disk.

Referring to the Fig. (2), the impacting forces, in the inertial system (x,y) can be calculated as:

$$F_n = \left\{ K_C \left(R-\delta\right) + C_C \frac{d}{dt}\left(R-\delta\right) \right\} H_{(R-\delta)}$$

Where $\mathbf{R}_0 = \begin{bmatrix} x & y \end{bmatrix}^T$ and $\mathbf{R}_c = \begin{bmatrix} X & Y \end{bmatrix}^T$ are the disk and the annular ring center coordinates, respectively; $R = \sqrt{(x-X)^2 + (y-Y)^2}$ is the radial displacement of the disk center, and, $H_{(\bullet)}$ is the Heavyside function.

The impact force components in the coordinate system (x,y), and, the torque generated by the tangential impact force, can be written as:

$$\begin{bmatrix} F_x \\ F_y \end{bmatrix} = \left(\frac{F_n}{R}\right) \begin{bmatrix} +(y-Y) & -(x-X) \\ -(x-X) & -(y-Y) \end{bmatrix} \begin{bmatrix} \mu \\ 1 \end{bmatrix}; \; T_t = -F_t R_d$$

Finally, the generalized forces ***Q*** corresponding to the external forces, acting on the disk, are given by:

$$\mathbf{Q} = \begin{bmatrix} Q_x & Q_y & Q_\theta & Q_\phi \end{bmatrix}^T = \begin{bmatrix} F_x & F_y & T_m & T_t \end{bmatrix}^T$$

Here, $T_m$ represents the torque acting on the rotor, that was encountered experimentally, and is described by a polynomial function:

$T_m = C\left[-0.002441\left(\frac{\Omega}{C}\right)^3 + 0.177\left(\frac{\Omega}{C}\right)^2 - 5.608\left(\frac{\Omega}{C}\right) + 290.65\right]$ N-mm, where $C = \frac{150}{66}$ is a constant and $\Omega$ (rad/s) is the rotor's rotational speed.

### 2.3. Full Annular Rubbing

For an unbalanced disk, when it does full annular rubbing, the centrifugal force generated by the imbalance ($m_\varepsilon$) may be greater or minor than the restoring force. If it is greater, the tangential friction force tends to accelerate the disk in the opposite direction of its rotating direction. If there is an unlimited energy supply through the motor, the acceleration may not stop until the relative velocity between the disk and ring becomes zero, in this condition, the disk will roll on the ring inner surface.

#### 2.3.1. Forward and Backward Whirl

In order to realize if the disk is doing forward or backward whirl, we define an angular displacement $\psi$, as it is showed in the Fig. (3), therefore, we can write the relationship: $\tan(\psi) = \frac{y}{x} \rightarrow \psi = \text{atan}(\frac{y}{x})$ and its derivative as:

$$\dot{\psi} = \frac{x\dot{y} - \dot{x}y}{x^2 + y^2} \tag{12}$$

Fig. (3) shows the same direction for $\dot{\psi}$ and $\Omega$, then, if $\dot{\psi}$ results positive, the disk is doing forward whirl, otherwise the disk is doing backward whirl.

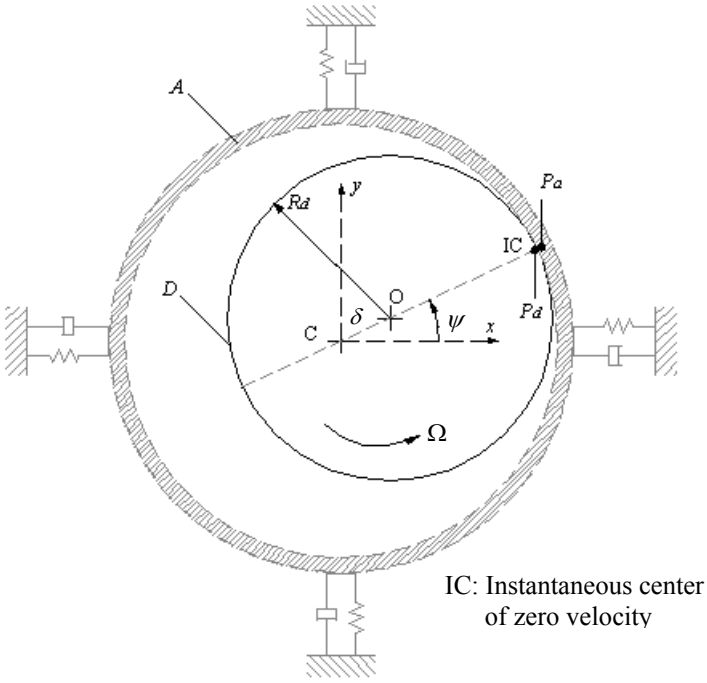


Figure 3. Full annular rubbing.

#### 2.3.2. Rolling and Sliding

In Fig. (3), consider two rigid bodies *A* and *D* in movement, such that, for each instant, there is a point $P_a \in A$ in contact with another point $P_d \in D$. Then, there exists rolling between *A* and *D*, for any reference (*S*), if the relative velocity between $P_a$ and $P_d$ is zero, mathematically this is expressed as: ${}_S\mathbf{V}_{P_a/P_d} = \mathbf{0}$. Taking a reference system (*S*) fixed at the annular ring, the velocity of point $P_d$, in the reference (*S*) is written as:

$$ {}_S\mathbf{V}_{P_d} = {}_S\mathbf{V}_O + \boldsymbol{\Omega}\times\mathbf{r}_{OP_d} \;\rightarrow\; {}_S\mathbf{V}_{P_d} = \dot{\psi}\hat{\mathbf{k}}\times\mathbf{r}_{CO} + \Omega\hat{\mathbf{k}}\times\mathbf{r}_{OP_d} \tag{13} $$

Also:

$$ {}_S\mathbf{V}_{P_a} = \mathbf{0} \;\rightarrow\; {}_S\mathbf{V}_{P_d} = \mathbf{0} $$

$$ \mathbf{r}_{CO} = \delta\cos\psi\,\hat{\mathbf{i}} + \delta\,\mathrm{sen}\,\psi\,\hat{\mathbf{j}};\quad \mathbf{r}_{OP_d} = R_d\cos\psi\,\hat{\mathbf{i}} + R_d\cos\psi\,\hat{\mathbf{j}} $$

Finally, Eq. (13) results:

$$ {}_S\mathbf{V}_{P_d} = (-\delta\dot{\psi}\,\mathrm{sen}\,\psi - R_d\Omega\,\mathrm{sen}\,\psi)\,\hat{\mathbf{i}} - (\delta\dot{\psi}\cos\psi + R_d\Omega\cos\psi)\,\hat{\mathbf{j}} = \mathbf{0} \tag{14} $$

For the rolling case we adopt the notation $\Omega_{wh} = \dot{\psi}$, that represents the whirl velocity with pure rolling, therefore, the kinematic condition for rolling is given by Eq. (15), if this equation is not satisfied, the rotor is sliding.

$$ \Omega_{wh} = -\frac{R_d}{\delta}\Omega \tag{15} $$

## 3. Experimental Test Rig

In order to investigate if the mathematical model can describe the behavior of the system, it was necessary to set up a test rig. It was build at the Dynamics and Vibration Laboratory of PUC-Rio. The test rig has electric and mechanic components and electronic devices for a correct data acquisition. In Fig. (4) it is showed a test rig photo with its components.

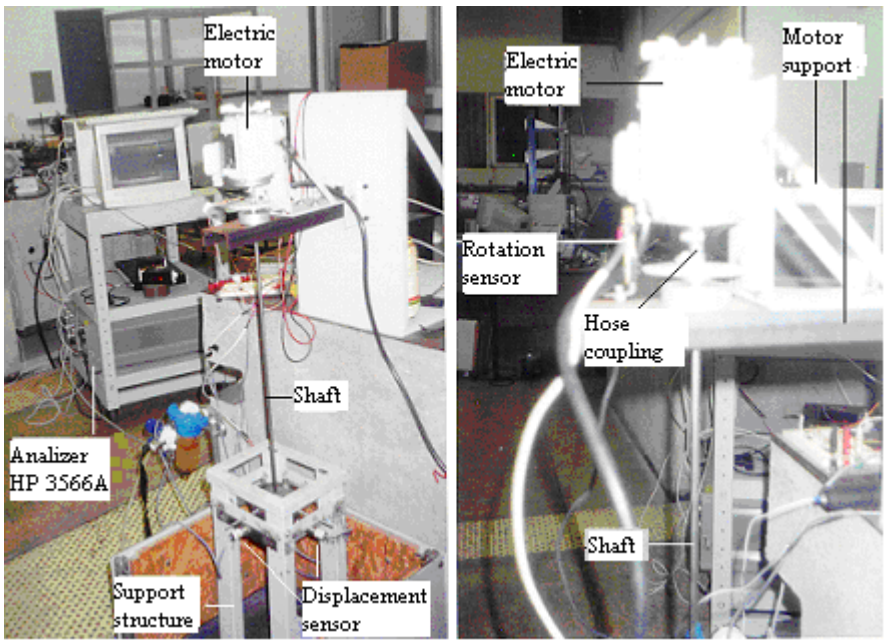


Figure 4. Test rig.

As is shown in Fig. (4), the main components are: a steel shaft $\phi$ 8x1000mm, a steel disk $\phi$ 100mm and thickness 40mm, steel annular ring with $\phi_i$ 101.8mm and $\phi_O$ 113.8, a base structure which supports the ring, an electric motor with frequency inverter, displacement and rotating sensors, etc. For data acquisition it was used an HP-3566A analyzer.

## 4. Numerical Simulation and Experimental Results

In order to solve, numerically, the motion equation given by Eq. (11), here it is used the 5$^{th}$ order Runge-Kutta Fehlberg method with variable step, Kreyszig (1999). This method for integration is better than others, because it is capable to calculate the error that serves as a step control. For all numerical simulations zero initial conditions are assumed, i.e. the initial disk center position coincides with the shaft motor center, and, the disk velocity is zero. Also, in Table (1) there are given numerical values for the simulation, some of them were calculated from the experimental test rig, and, other were taken from the literature review.

Table 1 – Some geometrical and physical parameters for the rotor dynamic system

| | | | |
|---|---|---|---|
| **Disk** | | | |
| Mass | $m_d$ | 2.5 | kg |
| Radio | $R_d$ | 50.0 | mm |
| **Annular Ring** | | | |
| Mass | $m_e$ | 0.38 | kg |
| Inner radio | $R_e$ | 50.9 | mm |
| **Shaft** | | | |
| Diameter, Length | $d$ , $L$ | 8.0, 620.0 | mm |
| Flexural stiffness | $K_b$ | 506.1 | N/m |
| Torsional stiffness | $K_t$ | 51.8 | N-m/rad |
| Torsional and flexural damping factor | $c_t$ , $c_b$ | 0.01, 0.01 | |
| **Contact parameters** | | | |
| Contact stiffness | $K_c$ | $1.0\text{x}10^6$ | N/m |
| Contact damping coefficient | $C_c$ | 0.1 | N-s/m |
| **Eccentricity** | | | |
| Mass | $m_\varepsilon$ | 0.03 | kg |
| Coordinate | $(\varepsilon_x, \varepsilon_y)$ | $(28.2, 28.2)$ | mm |

### 4.1. Rotor with Acceleration – Numerical Simulation

For this simulation, the disk behavior is analyzed for two cases: without and with the annular ring of the rotor system. The results without the ring are showed in Fig. (5), it is a typical dynamical system behavior passing through its critical speed ( $\omega_c = 2.29$ Hz.). Firstly the disk orbit starts at the point (0,0), while the disk is accelerating due to the motor torque, the disk orbit grows, after reaching the maximum orbit amplitude (near its critical speed), the disk orbit decreases until it reaches the steady-state motion. Fig. (5) shows clearly that the frequency where there occurs the maximum orbit amplitude is moving to the right side of the critical speed, when the torque is increasing. The new frequencies for the maximum orbit are 1.16( $\omega_c$ ), 1.53( $\omega_c$ ) and 3.10( $\omega_c$ ) Hz for the 1%, 10% and 100% $T_m$ , respectively. This behavior is also named by Childs (1993) and Markert & Seidler (2001).

On the other hand, let us now consider the annular ring in the rotor system and apply a 100% $T_m$ . In this case, the radial gap between the ring and the disk is considered 0.9mm; therefore, it is expected that the disk impact the ring, since it will restrict its free motion. In Fig. (6) it is shown the disk orbit for two different values of the friction coefficient $\mu$ (0.01 and 0.2). There, we can see that for a low friction coefficient ( $\mu = 0.01$ ), the disk, after some impacts, is moving in a forward whirl form; on the other hand, when the friction coefficient is high ( $\mu = 0.2$ ) the backward whirl motion is occurring.

### 4.2. Rotor with Constant Rotational Velocity – Numerical Simulations

For this simulation, the disk behavior is analyzed when the rotor is operating at constant rotational velocity, for the numerical simulation, the nominal velocity is assumed $\Omega = 2.29$ Hz. Again, the radial gap is settled as 0.9mm. Fig. (7) shows the disk orbit and, it also shows that for low friction coefficient the disk is doing forward whirl and for high friction coefficient the backward whirl is occurring. This same behavior also was pointed out by Bartha (2001), who observed a strong dependence of the friction coefficient to induce the whirl phenomena in the disk.

### 4.3. Rotor with Constant Rotational Velocity – Experimental Results

In this item, we show experimental results from the test rig for two rotor rotations, an imbalance mass $m_\varepsilon = 9.3$ gr. and a single radial gap (0.9mm). Figure (8a) shows that the disk develops forward whirl when the surfaces in contact have low friction coefficient (greased surfaces), and, it develops backward whirl motion, Fig. (8b), when the friction coefficient is high, (dry surfaces).

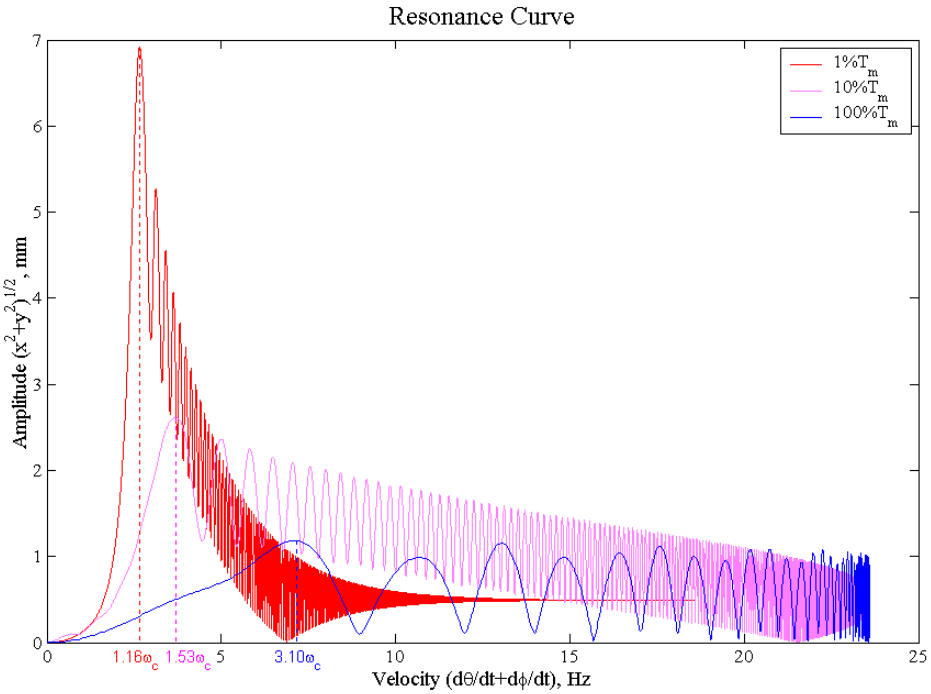


Figure 5. Resonance curve for three different motor torques.

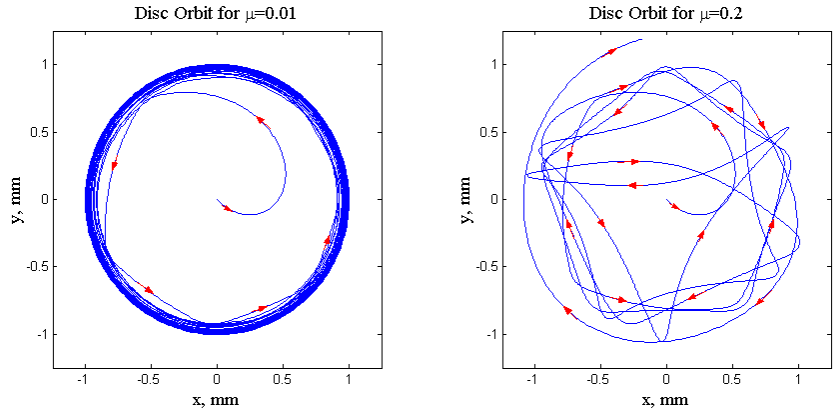


Figure 6. Disk orbit for different $\mu$ – accelerating rotor (left: forward whirl, right: backward whirl).

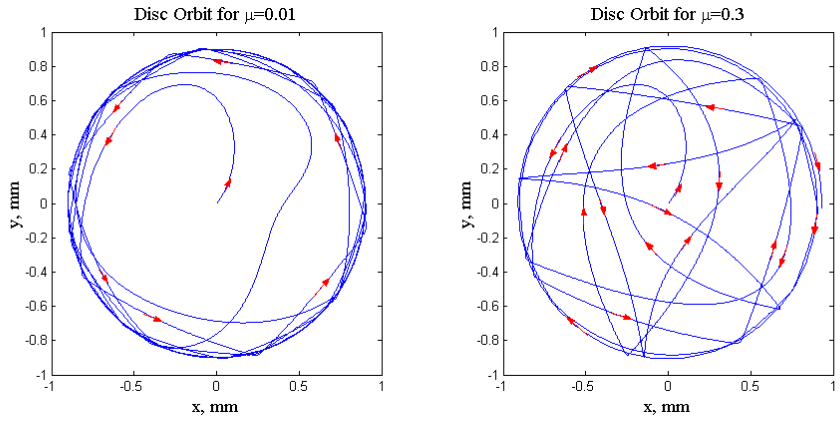


Figure 7. Disk orbit for different $\mu$ – constant rotational velocity (left: forward whirl, right: backward whirl).

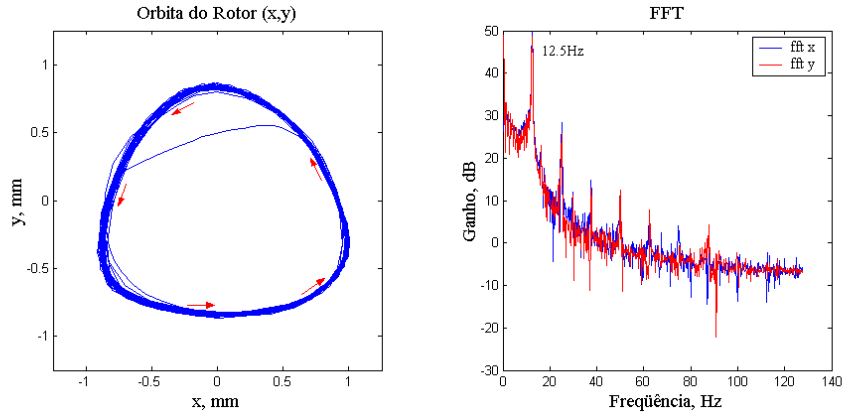


Figure 8a. Disk orbit for greased surfaces – Forward whirl (Motor speed 7.0Hz).

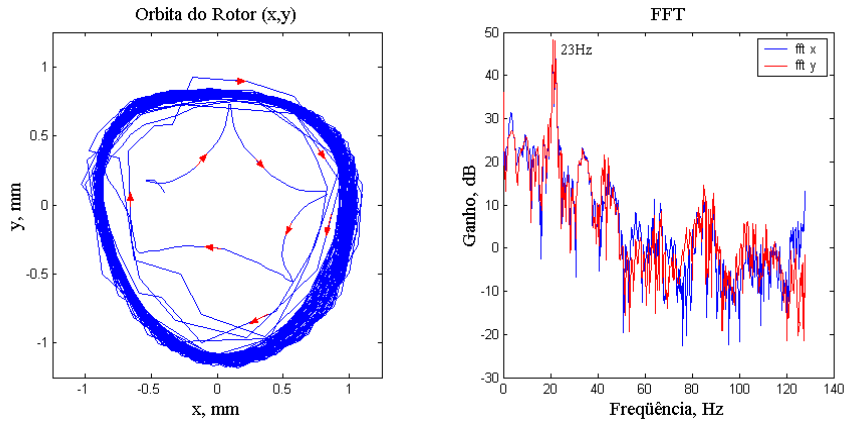


Figure 8b. Disk orbit for dry surfaces – Backward whirl (Motor speed 12.0Hz).

## 5. Comparison with Experiments

For a first experiment the surfaces in contact are dry (high friction coefficient) and in another experiment the surfaces were greased to reduce $\mu$ (low friction coefficient).

Numerical results, Fig. (7), show us the forward whirl motion for $\mu = 0.01$ and a backward whirl motion for $\mu = 0.3$. This same behavior, qualitatively, is obtained experimentally, Fig. (8). In the experimental results, we can see that for low friction coefficient, the disk orbit is smoother than for high friction coefficient. An FFT of this orbits give us two frequencies: 23Hz for backward and 12.5Hz for forward whirl. The backward whirl frequency always is higher because in the rolling condition the radial gap is lower than the disk radio, $\delta << R_d$, Muszynska (1984). In our experimental results the rotor is slipping since the frequency of backward whirl for rolling ($\Omega_{wh} = -\frac{R_d}{\delta}\Omega$) is not obtained in the experiment. The whirl frequencies in rolling condition for each experimental test, using Eq. (15), are: $|\Omega_{wh}| \approx 667\text{Hz}$ (for motor speed 12Hz) and $|\Omega_{wh}| \approx 389\text{Hz}$ (for motor speed 7Hz).

The same kind of behavior encountered in this work, was obtained by Melakhessou et al. (2003), they used an stator covered with rubber to get high friction coefficient in they test rig.

## 6. Conclusions

In this work the dynamics of a vertical overhung rotating system was analyzed. This model can represent satisfactorily the lateral dynamics of a drillstring section in oil well drilling. The proposed model takes into account the impact phenomena, which occurred between a drillstring section and well-bore. Through the numerical and experimental results obtained we can conclude that the model is suitable and accurate to simulate the local behavior of the drillstring at a contact section.

The study of the rotating system includes the free passing through its critical speed and the motion when an annular ring limits the disk. When it is passing its critical speed, we found out that the frequency where the maximum orbit amplitude occurs is varying with the torque on the rotor; for higher torques the new frequencies moves to the right side of the critical speed. Also, it is necessary to point out that when there is low damping in the system, as used for the

numerical simulation, the transient don't dies away in the resonance curves and the solution of the system looks like the obtained curve.

This work shows that there is a strong dependence of the friction coefficient to induce the whirl movement. For low friction coefficient, the disk develops forward whirl, and, backward whirl when the friction coefficient is high. This result was verified experimentally in the test rig. In the process of validation of the developed model, one interesting conclusion is that the backward whirl can be avoided decreasing the amount of friction present at the surfaces that get in contact.

From the numerical point of view, the use of only one equation to analyze the several types of possible motions, with and without contact is shown leading to results with a good precision and convenient CPU time.

## 7. References


Atalla, M. J. "Estudo Fenomenologico do Diagrama de Campbell em Sistemas Rotativos com Poucos Graus de Liberdade", Universidade Estadual de Campinas, Iniciação Cientifica, 1991.

Bartha, A. R. "Dry Friction Backward Whirl of Rotors", Diss., Technische Wissenschaften ETH Zürich, Nr. 13817, 2001.

Brach, R. M. "Formulation of Rigid Body Impact Problems Using Generalized Coefficients", Int. J. Engng Sci. Vol. 36, No. 1, pp. 61-71, 1998.

Childs, D. "Turbomachinery Rotordynamics", Phenomena, Modeling, and Analysis, John Wiley & Sons, Inc., 1993.

Jansen, J. D. "Nonlinear Dynamics of Oilwell Drillstrings", Delft University Press, 1993.

Markert, R. and Seidler, M. "Analytically Based Estimation of the Maximum Amplitude During Passage Through Resonance", International Journal of Solids and Structures 38 (2001) 1975-1992.

Melakhessou, H. and Guy A. B. "A Nonlinear Well-Drillstring Interaction Model", Transactions of the ASME, Journal of Vibration and Acoustics, January 2003, Vol. 125, pag. 46-52.

Muszynska, A. "Partial Lateral Rotor to Stator Rubs", ImechE Conference Transactions C281/84, Mechanical Engineering Publications, London, 1984.

Rajalingham, C. and Rakheja, S. "Analysis of Impact Force Variation During Collision of Two Bodies Using a Single Degree of Freedom System Model", Journal of Sound and Vibration (2000) 229(4), 823-835.

Schiehlen, W. and Seifried, R. "Impact Models: From Wave Propagation to Body Motion", X DINAME, Ubatuba, SP - Brazil, (2003), pg. 77-81.